Inorganic Chemistry

Article

pubs.acs.org/IC

Synthesis, Crystal Structure, and High-Temperature Phase Transition of the Novel Plumbide Na_2MgPb

Takahiro Yamada,*[,†] Takuji Ikeda,[‡] Ralf P. Stoffel,[§] Volker L. Deringer,[§] Richard Dronskowski,[§,∥] and Hisanori Yamane[†]

[†]Institute of Multidisciplinary Research for Advanced Materials, Tohoku University, 2-1-1 Katahira, Aoba-ku, Sendai 980-8577, Japan

[‡]Research Center for Compact Chemical System, National Institute of Advanced Industrial Science and Technology (AIST), 4-2-1 Nigatake, Miyagino-ku, Sendai 983-8551, Japan

[§]Institute of Inorganic Chemistry, RWTH Aachen University, Landoltweg 1, 52056 Aachen, Germany

[∥]Jülich−Aachen Research Alliance (JARA-HPC), RWTH Aachen University, Landoltweg 1, 52056 Aachen, Germany

Supporting Information

ABSTRACT: A hitherto unknown sodium magnesium plumbide, Na_2MgPb, was synthesized by heating the constituent elements. Na_2MgPb crystallizes in a hexagonal unit cell with the Li_2CuAs-type structure ($P6_3/mmc$, $Z = 2$, $a = 5.110(2)$ Å, $c = 10.171(4)$ Å at 293 K). The compound furthermore displays polymorphism: high-temperature powder XRD measurements revealed that hexagonal Na_2MgPb (dubbed the "α" phase) transforms to another hexagonal phase (β) which is existent at 493−553 K, and the β phase changes to a cubic structure (γ) at 533−633 K further. The molar volume of γ-Na_2MgPb is approximately 9% and 13% smaller than the molar volumes of the α phase and the β phase, respectively (at 543 K). The electrical resistivity of Na_2MgPb is 0.39 mΩ at 300 K; it rises with increasing temperature from 300 to 491 K, and then drops at 491 and 523 K. These abrupt changes in resistivity may be attributed to the $\alpha \rightarrow \beta$ and $\beta \rightarrow \gamma$ phase transitions, respectively. To gain further insight into the structure of cubic γ-Na_2MgPb, putative models with regular Heusler-type (Cu_2MnAl-type) and inverse Heusler-type (Li_2AgSb-type) arrangements were probed using first-principles computations based on density functional theory (DFT). These computations indicate that, for the cubic γ phase, an inverse Heusler-type structure is distinctly more stable than the alternative regular Heusler type (at 0 K); beyond that, *ab initio* thermochemistry was successfully used to verify the stability ordering (α-Na_2MgPb being favorable at low temperature, γ-Na_2MgPb at high temperature), albeit the theoretically predicted transition temperature of 900 K which is higher than observed in experiment.

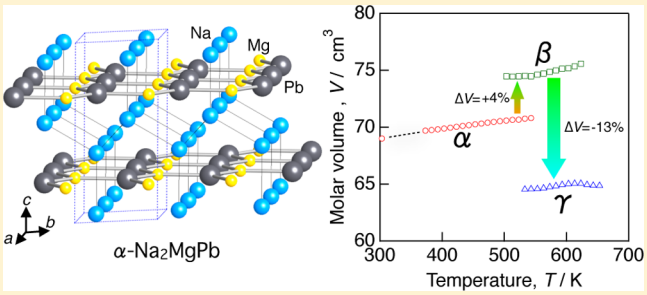

1. INTRODUCTION

Eight crystal structure types have been reported for intermetallic compounds with the general formula A_2MeTt, where A denotes an alkali metal (Li, Na, K), Me is a group-12 element (Zn, Cd, Hg), and Tt stands for one of the tetrels (Si, Ge, Sn, Pb).[1−13] These solid-state phases are known for their structural versatility: Me and Tt atoms may connect in those structures to form one-dimensional (1D) chains (K_2CdSn-type and Na_2CuAs-type), two-dimensional (2D) layers (Li_2CuAs-type and Li_2ZnSi-type), and also three-dimensional (3D) frameworks; the latter are seen in the inverse Heusler-type (Li_2AgSb-type), the regular Heusler-type (Cu_2MnAl-type), as well as the Na_3As- and Li_3Bi-type. In these structures, the alkali metal atoms (A) are located between the chains and layers, or within structural voids in the Me/Tt frameworks. For example, Na_2CdSn[9] adopts the hexagonal Li_2CuAs structure type and thus contains 2D honeycomb Cd−Sn layers, whereas the heavier analogue Na_2CdPb[9] exhibits a 3D Cd−Pb framework, as it crystallizes in the inverse Heusler type. The latter structure type was also reported for Li_2CdPb[5] and Li_2CdSn.[7] Furthermore, Li_2CdSn exhibits a polymorph with the regular Heusler-type structure.[2]

Besides the compounds A_2MeTt with Me = group-12 elements, there have also been successful syntheses of Li_2MgTt compounds (Tt = Ge, Sn, and Pb) with regular Heusler-type structures.[14,15] Besides that, Li_2MgSn has a polymorph with the NaTl-type structure.[16] The structures analyzed for the two polymorphs of Li_2MgSi are the inverse Heusler-type and Li_2MgSi-type.[17,18] The Li_2MgSi-type and NaTl-type structures are not included in the eight structure types of A_2MeTt compounds.

Recently, Yamada et al. synthesized a stannide Na_2MgSn,[19] which constituted the first ternary compound in the Na−Mg−Sn system. It crystallizes in the Li_2CuAs-type structure (hexagonal, $P6_3/mmc$, $Z = 2$, $a = 5.0486(11)$ Å, $c =$

Received: February 27, 2014
Published: May 2, 2014

   dx.doi.org/10.1021/ic500466w | *Inorg. Chem.* 2014, 53, 5253−5259

10.095(2) Å) with two-dimensional honeycomb layers of $^{2}_{\infty}[(MgSn)^{2-}]$. Electrical resistivity measurements for Na_2MgSn revealed p-type semiconducting behavior with a narrow energy gap of 0.17 eV. It would now seem rewarding to attempt a substitution of Sn with the heavier homologue Pb, in search of a ternary Na_2MgPb compound.[19] In the present Article, we describe the successful synthesis of Na_2MgPb and its crystal structure elucidation by means of single-crystal X-ray diffraction (XRD). Interestingly, Na_2MgPb exhibits polymorphism and thus undergoes two subsequent structural phase transitions upon heating. The latter have been investigated using a combination of variable-temperature powder XRD, electrical conductivity measurements at high temperature, and state-of-the-art density-functional theory (DFT) and *ab initio* thermochemical computations.

2. EXPERIMENTAL AND COMPUTATIONAL METHODS

Synthesis. The manipulation of elemental sodium and of the obtained samples, all of which are unstable in air, were carried out in an argon-filled glovebox (MBraun; O_2, H_2O < 1 ppm). Elemental Na (lump, 99.95%, Nippon Soda Co. Ltd.), Mg (rod, 1.5 mm diameter, 99.98%, The Nilaco Co., Ltd.), and Pb (shot, 99.99%, Wako Pure Chemical Industries, Ltd.) were weighed in the desired molar ratio. A sintered BN crucible (inside diameter 6 mm; depth 18 mm in inner volume, Showa Denko, 99.5%) was loaded with the source elements (approximately 0.5 g in total) and sealed in a stainless steel tube (SUS316, an inner diameter of 10.5 mm, a length of 90 mm) with stainless steel caps. The source elements with a molar ratio of Na:Mg:Pb = 2:1:1 were heated at 973 K for 2 h and then at 823 K for 12 h. After cooling, a polycrystalline bulk ingot was obtained. Single crystals of Na_2MgPb were obtained from the ingot, in which Na_2MgPb was the main phase. Another ingot was prepared with a slightly different ratio of the source elements, namely, Na:Mg:Pb = 2.26:1.09:1.00; the latter sample was pulverized with an agate mortar. The obtained powder was then pressed into a compact sample (ca. 14 × 3 × 2 mm^3) which was sintered at 773 K for 10 h in Ar atmosphere for subsequent electrical-conductivity measurements of Na_2MgPb.

Chemical Analysis. The contents of Na, Mg, and Pb in the sample were analyzed using inductively coupled plasma optical emission spectroscopy (ICP-OES, Model: SPECTRO Arcos, SPECTRO Analytical Instruments, Germany).

Structure Elucidation. The powder X-ray diffraction (XRD) pattern of Na_2MgPb was collected under argon atmosphere at room temperature on a modified Debye–Scherrer-type diffractometer (Bruker D8-Advance) using Cu $K\alpha_1$ radiation with a primary Ge(111) monochromator and a linear position-sensitive VÅNTEC-1 detector. The measurement temperature range was from 303 to 653 K. For obtaining accurate crystal structure data, the XRD data of a Na_2MgPb single crystal sealed in a glass capillary were collected using Mo Kα radiation with a graphite monochromator and an imaging plate on a single-crystal X-ray diffractometer (Rigaku, R-AXIS RAPID-II). X-ray diffraction data collection and unit-cell refinement were performed by the PROCESS-AUTO program.[20] An analytical absorption correction was applied by the NUMABS program.[21] The crystal structure was refined by full-matrix least-squares on F^2 with the aid of the SHELXL-97 program.[22] All calculations were carried out on a personal computer using the WinGX software package.[23] The atomic coordinates were standardized by the STRUCTURE TIDY program.[24]

Electrical Properties. After sintering at 773 K, the electrical resistivity of the polycrystalline sample was measured in Ar atmosphere by a direct current four-probe method in the temperature range 300–743 K. The measured sample had a relative density of approximately 70% of the theoretical density of Na_2MgPb.

Quantum Chemistry. Density-functional theory (DFT) based electronic-structure computations were carried out using the Vienna *ab Initio* Simulation package (VASP).[25] The electronic ground state energy as well as temperature-dependent electronic energy contributions were calculated using VASP,[26,27] employing plane-wave basis sets with kinetic energy up to 500 eV together with the projector augmented-wave method.[28] Exchange and correlation were treated following the parametrization of Perdew, Burke, and Ernzerhof.[29] In order to sample the Brillouin zone the tetrahedron method with Blöchl's correction was used,[30] together with a dense mesh of *k*-points,[31] which resulted in at least 2500 *k*-points × atoms.

Phonon properties were calculated following the *ab initio* force constant method[32] as implemented in the fropho code.[33] The thermodynamic functions were evaluated in the framework of the quasiharmonic approximation as described in ref 34. To do so, the Helmholtz free energy was first obtained as the sum of the electronic ground state energy, the temperature-dependent electronic excitational energies (see above), and the harmonic vibrational (phonon) free energy at given temperatures and volumes. In a second step, the Gibbs free energy $G = A + pV$ was extracted from a set of constant-volume phonon computations by deriving the pressure from standard thermochemical relations, that is, $p = A - (\partial A/\partial V)_T$.

3. RESULTS AND DISCUSSION

3.1. X-ray Single-Crystal Structural Analysis of α-Na_2MgPb. Single crystals were picked up from a crushed sample that had been prepared by heating the source elements with a molar ratio of Na:Mg:Pb = 2:1:1 at 973 K for 2 h and 823 K for 12 h. Because the crystals were unstable in air, the single-crystal XRD measurement was performed for a crystal sealed in a glass capillary. The single-crystal XRD reflections were indexed with a hexagonal unit cell with lattice parameters of a = 5.110(2) Å and c = 10.171(4) Å. The observed extinction conditions were compatible with space group $P6_3/mmc$ (No. 194) which is identical to that of Na_2MgSn.[19] Structural refinement was conducted using an initial structural model in which the Sn atom of Na_2MgSn was substituted by Pb; i.e., Na rests on the Wyckoff position 4*f* ($^1/_3$, $^2/_3$, *z*), Mg on 2*b* (0, 0, $^1/_4$), and Sn on 2*c* ($^1/_3$, $^2/_3$, $^1/_4$). The final refinement resulted in R1 = 0.046 and S = 1.09 for 2$\sigma(I)$ data, and the refined z coordinate of the Na atom was 0.5808(14). Details of the data collection and crystallographic information are summarized in Table 1. Atomic coordinates and anisotropic and isotropic displacement parameters are given in Table 2, and selected bond lengths and angles are listed in the Supporting Information (Table S1).

Figure 1 shows the crystal structure of Na_2MgPb (which is here dubbed α phase; see below) with the Li_2CuAs-type structure, which is isostructral with Na_2MgSn and Na_2CdSn;[9] it should be noted that, in the latter case, the equivalent plumbide Na_2CdPb[9] crystallizes in the inverse Heusler-type structure with $F\bar{4}3m$ cubic symmetry. In Na_2MgPb, honeycomb lattice layers, formed by Mg (2*b* site) and Pb (2*c* site) atoms lying in the same plane, stack along the c axis, and Na atoms fill the space between the layers. The Na atoms are located above/below the centers of the hexagons of the closest honeycomb layer, forming a Lonsdaleite-type framework (see details in Supporting Information Figure S1). The shortest interatomic distances between Mg and Pb atoms in the layer and between Na atoms are 2.9503(7) and 3.377(10) Å, respectively, and the interlayer distance is 5.086(2) Å. These values are 0.8–1.2% larger than those of Na_2MgSn (d_{Mg-Sn} = 2.9148(3) Å, d_{Na-Na} = 3.329(3) Å, $d_{Mg-Sn\ layers}$ = 5.0475(10) Å)[19] due to the difference in atomic radii (Pb, 1.54 Å; Sn, 1.45 Å).[35]

3.2. Optimized Synthesis of Na_2MgPb Polycrystalline Sample. The sample prepared by heating the source materials with a molar ratio of Na:Mg:Pb = 2:1:1 was not a single phase of Na_2MgPb, containing some amount of unidentified phases. On the contrary, the polycrystalline sample of the α phase

dx.doi.org/10.1021/ic500466w | Inorg. Chem. 2014, 53, 5253–5259

Table 1. Crystal Data and Refinement Results for α-Na_2MgPb

chemical formula	Na_2MgPb
fw, M (g mol^{-1})	277.48
T (K)	293(2)
cryst syst	hexagonal
space group	$P6_3/mmc$ (No. 194)
unit cell dimensions (Å)	a = 5.110(2)
	c = 10.171(4)
unit cell volume, V (Å^3)	230.04 (16)
Z	2
calcd density, D_{cal} (Mg m^{-3})	4.01
radiation wavelength, λ (Å)	0.710 75
cryst form, color	fragment, silver-gray
abs corr	numerical
abs coeff, μ (mm^{-1})	36.77
cryst size (mm^3)	0.151 × 0.145 × 0.038
limiting indices	$-6 \le h \le 6$
	$-6 \le k \le 6$
	$-12 \le l \le 13$
F_{000}	232
θ range for data collection (deg)	4.01−27.47
reflns collected/unique	902/128
R_{int}	0.154
data/restraints/params	125/0/8
weight params, a, b	0.00, 2.9296
GOF on F^2, S	1.09
R1, wR2 ($I > 2\sigma(I)$)^{a,b}	0.046, 0.078
R1, wR2 (all data)^{a,b}	0.051, 0.080
largest diff peak and hole, $\Delta\rho$ (e Å^{-3})	0.90, −0.45

^{a}R1 = $\sum||F_o|| - ||F_c||/\sum||Fo||$. ^{b}wR2 = $\{[\sum w[(F_o)^2 - (F_c)^2]^2]/[\sum w(F_o^2)^2]\}^{1/2}$; $w = [\sigma^2(F_0)^2 + (AP)^2 + BP]^{-1}$, where $P = [(F_o)^2 + 2(F_c)^2]/3$.

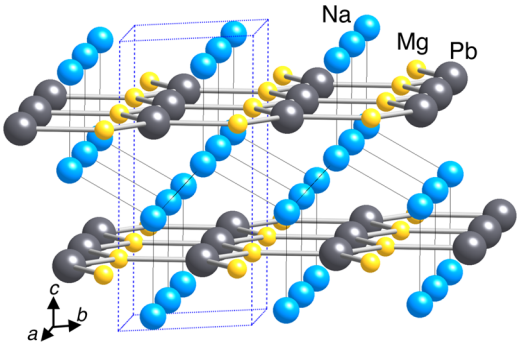

Figure 1. Schematic drawing of the hexagonal Li_2CuAs-type crystal structure of α-Na_2MgPb.

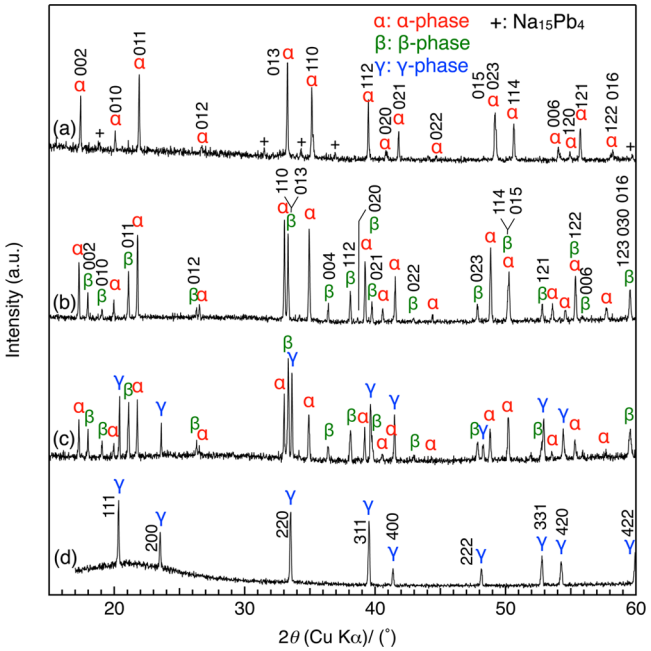

Figure 2. XRD patterns of Na_2MgPb at 303 K (a), 513 K (b), 543 K (c), and 653 K (d).

could be prepared from a mixture of the starting materials with an excess amount of Na and Mg (Na:Mg:Pb = 2.26:1.09:1.00). The powder XRD pattern of the latter product sample at 303 K is shown in Figure 2a. All peaks, except small peaks of $Na_{15}Pb_4$ as a second phase, were indexed in a hexagonal crystal system with unit cell parameters of a = 5.1019(4) Å, c = 10.1731(8) Å which were consistent with the cell parameters that had been measured using single-crystal XRD.

The improvement in product quality is understandable since the source elements Na and Mg have higher vapor pressures than Pb (Na, 1.33 × 10^4 Pa; Mg, 933 Pa; Pb, 0.8 Pa at 973 K).[36] The chemical composition of the prepared samples was slightly different from the starting composition of the source mixture due to evaporation of Na and/or Mg during heating; similar observations have been made before for Na_2MgSn.[19] The weight concentration of Na, Mg, and Pb in the polycrystalline Na_2MgPb sample analyzed by ICP-OES measurement was 17.4(1), 9.3(1), and 71.3(7) wt % (total: 98.0(9) wt %). The molar ratio of the metals in the sample was calculated to be 2.19(3):1.11(3):1 for Na:Mg:Pb. It was not very different from the molar ratio of the source materials (2.26:1.09:1) for the Na_2MgPb sample preparation.

3.3. High-Temperature XRD Measurement. The powder XRD patterns measured at 513, 543, and 653 K for the samples are shown in Figure 2b−d. In the pattern recorded at 513 K, besides the peaks of Na_2MgPb with the hexagonal Li_2CuAs-type structure (α phase), several additional peaks were observed and indexed with hexagonal unit cell parameters of a = 5.3800(5) Å and c = 9.8772(13) Å. The latter hexagonal phase which appeared at 513 K is hereafter referred to as β-Na_2MgPb. At 543 K, additional peaks were observed and indexed with a cubic unit cell parameter of a = 7.5408(1) Å, besides the still existent peaks of the α and β phases. Finally, in

Table 2. Atomic Coordinates and Anisotropic and Isotropic Displacement Parameters[a]

atom	site	x	y	z	U_{11}(Å^2)	U_{33}(Å^2)	U_{12}(Å^2)	U_{eq} (Å^2)
Na	4f	$^1/_3$	$^2/_3$	0.5808(14)	0.041(4)	0.061(10)	0.0207(18)	0.048(3)
Mg	2b	0	0	$^1/_4$	0.017(3)	0.0067(9)	0.0083(13)	0.033(3)
Pb	2c	$^1/_3$	$^2/_3$	$^1/_4$	0.0287(5)	0.0426(9)	0.0144(3)	0.0334(5)

$^a U_{11} = U_{22}$, $U_{23} = U_{13} = 0$, $U_{eq} = (\sum_i\sum_j U_{ij}a_i^*a_j^*a_i{\cdot}a_j)/3$.

dx.doi.org/10.1021/ic500466w | Inorg. Chem. 2014, 53, 5253−5259

the XRD pattern at 653 K, only the peaks of the cubic phase (γ-Na_2MgPb) were observed.

In order to investigate the phase transition in more detail, the powder XRD measurement of the sample was performed from 373 to 653 K in 10 K increments in the range 2θ = 32°−42°. The measured XRD patterns are shown in Figure 3. The XRD

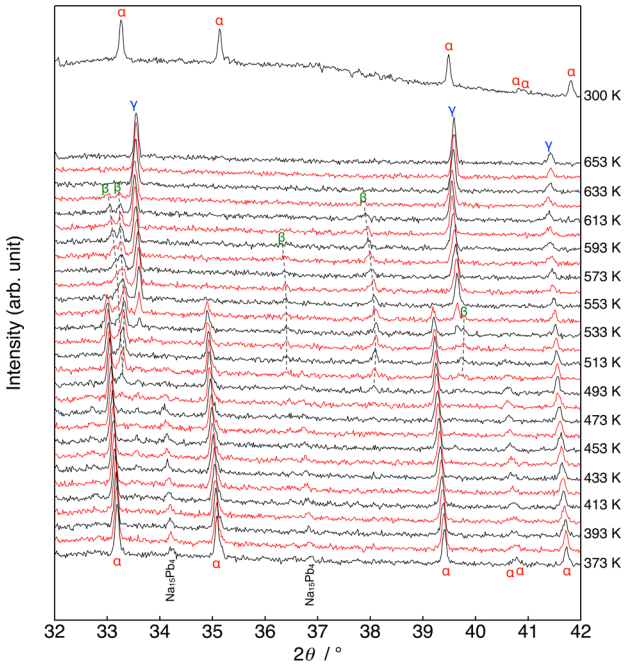

Figure 3. XRD patterns of Na_2MgPb at the temperatures from 373 K (bottom) to 653 K in 10 K increments and at 300 K (top) after cooling.

peaks of the α phase observed from 373 to 543 K shifted to lower angles. The intensities of the α phase peaks were significantly reduced above 513 K and could not been seen at and above 553 K. The 011 and 013, 004, 112, and 021 peaks of the β phase were observed at 33.3°, 36.4°, 38.1°, and 39.7°, respectively, at 493−503 K. The peak intensities increased with rising temperature and reached a maximum at 553 K, and then gradually decreased to zero at 633 K. The diffraction peaks of 220, 311, and 400 of the γ phase were observed above 553 K, and the peak intensities got larger with increasing temperature. After heating, the sample was cooled to 300 K, and the crystalline α phase was found at that temperature. These results indicate that the phase transition of the hexagonal α phase to the hexagonal β phase occurred at 493−553 K, and the β phase to the cubic γ phase at 533−633 K; finally, the γ phase reversibly returns to the α phase upon cooling down from 653 K. The γ phase could not be obtained by quenching from 653 K to room temperature.

The high-temperature X-ray diffraction data showed that the β phase cannot be obtained as a single phase. The β phase existed with the α phase from 493 to 543 K (temperature width of 50 K), and after disappearance of the α phase, it still existed with the γ phase from 553 to 623 K (temperature width of 70 K). Thus, the β phase must be an intermediate phase of the phase transition from α to γ. Such large temperature width of about 50 and 70 K observed by high-temperature XRD analysis may suggest that the phase transitions from α to β and β to γ are athermal and diffusionless (martensitic).

The lattice parameters of the α, β, and γ phases calculated from the high-temperature XRD data are shown in Figure 4a.

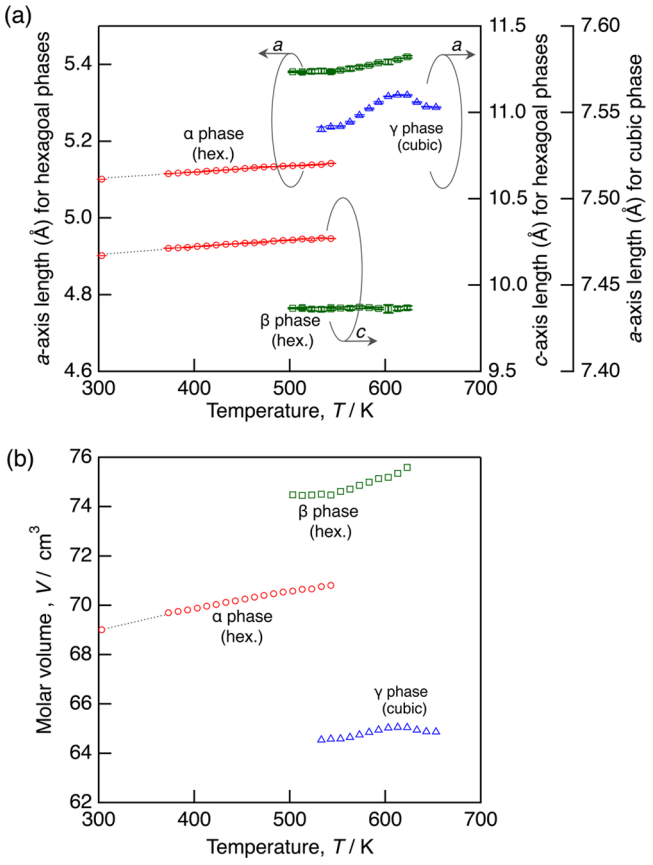

Figure 4. Lattice parameters (a) and molar volume (b) of the hexagonal α-Na_2MgPb (○) and β-Na_2MgPb (□), and cubic γ-Na_2MgPb (△) as a function of the temperature.

The a- and c-axis lengths of the α phase monotonically increased with increasing temperature, and the increments were +0.5% for the a-axis length (5.1116(6)−5.14213(5) Å) and +0.6% for the c-axis length (10.214(14)−10.270(17) Å) from the temperature range 373−543 K. The a- and c-axis lengths of the β phase were ca. 5% larger and 4% smaller, respectively, than those of the α phase at the same temperatures (505−543 K). The a-axis length of the β phase increased by +0.7%, while the c-axis length was almost constant (±0.1%) from 493 to 623 K. The lattice parameter (a-axis length) of the γ-phase increased by +0.3% (7.5403(14)−7.5600(4) Å) from 533 to 623 K, and then decreased to 7.5529(4) Å at 653 K.

At 543 K, where all three phases (α-, β-, and γ-Na_2MgPb) coexist, the molar volume of the γ phase is 64.6 cm^3 mol^{-1}, which is 9% and 13% smaller than that of the α phase (70.8 cm^3 mol^{-1}) and the β phase (74.5 cm^3 mol^{-1}), respectively (Figure 4b). In the A_2MeTt compounds mentioned in the Introduction, a comparable large volume shrinkage over −15% has been observed during the phase transition of Li_2ZnGe from the low-temperature phase with the hexagonal Na_3As-type structure (or the trigonal modified Na_3As-type structure) to the high-temperature phase with the cubic Li_3Bi type structure at 775−780 K.[2,3,10,11]

The extinction conditions of the powder XRD pattern of the hexagonal β-phase lead to the possible space groups $P6_3/mmc$ (No. 194), $P\bar{6}2c$ (No. 190), and $P6_3mc$ (No. 186). Of these

dx.doi.org/10.1021/ic500466w | Inorg. Chem. 2014, 53, 5253−5259

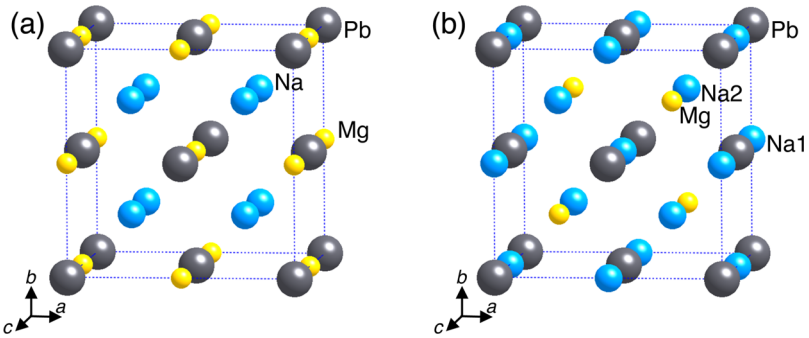

Figure 5. Schematic drawing of the regular Heusler-type structure model (a) and the inverse Heusler-type structure model (b) for the γ-Na_2MgPb phase.

Table 3. Atomic Coordinatiotes of γ-Na_2MgPb with the Regular and Inverse Heusler-type Structures

regular Heusler-type structure, $Fm\bar{3}m$					inverse Heusler-type structure, $F\bar{4}3m$				
site	Wyckoff position	x	y	z	site	Wyckoff position	x	y	z
Na	8c	$^1/_4$	$^1/_4$	$^1/_4$	Na1	8c	$^1/_2$	$^1/_2$	$^1/_2$
Mg	4b	$^1/_2$	$^1/_2$	$^1/_2$	Na2	4c	$^1/_4$	$^1/_4$	$^1/_4$
Pb	4a	0	0	0	Mg	4b	$^3/_4$	$^3/_4$	$^3/_4$
					Pb	4a	0	0	0

space groups, $P6_3/mmc$ is found in the A_2MeTt compounds Na_2CdSn[9] and Na_2MgSn[19] with the Li_2CuAs-type structure, and in Li_2ZnGe[10] with the Na_3As-type structure. However, the crystal structure of the β phase could not be determined in the present study.

For the cubic γ phase, there are five possible space groups ($Fm\bar{3}m$, $F\bar{4}3m$, $F432$, $Fm\bar{3}$, and $F23$) according to the systematic extinction of the powder XRD reflections observed. Among the previously reported A_2MeTt and $LiMgTt$ compounds, Li_2ZnSi and eight other compounds[2,3,6,37] crystallize in cubic cells with the regular Heusler-type structure ($Fm\bar{3}m$), whereas Na_2CdPb and eight other compounds[5,7,9,12] take the inverse Heusler-type structure ($F\bar{4}3m$). It seems reasonable to assume for the high-temperature γ phase either the regular Heusler-type structure or the inverse Heusler-type structure. Although, in principle, it is possible to distinguish between the regular and inverse type structures from the slight differences of the XRD peak intensities despite the similar scattering power of Na and Mg atoms, the crystal structure of γ-Na_2MgPb could not be determined unambiguously from the present high-temperature powder XRD data because the data quality was not good enough for the refinement.

3.4. Quantum-Chemical Computations. Theoretical computations based on density-functional theory (DFT) were performed to analyze the phase stabilities of the α phase with the Li_2CuAs-type structure and the γ phase, postulating for now that the γ phase should either take the regular Heusler-type or the inverse Heusler-type structure; both models are shown in Figure 5, and the corresponding atomic sites are listed in Table 3. All atoms of both structure types lie on special positions (Table 3); Na atoms are tetrahedrally surrounded by Pb atoms, and Mg atoms are octahedrally coordinated by Pb in the regular Heusler-type structure. In the inverse Heusler-type structural model, on the contrary, the octahedral sites are occupied by Na atoms whereas the tetrahedral sites are orderly occupied by Na and Mg atoms. It is difficult to distinguish one structure type from the other by powder XRD, due to the similar scattering power of Na and Mg atoms, as discussed before for Na_2MgSn.[19]

Figure 6a shows energy–volume data for the hexagonal α phase with the Li_2CuAs-type structure alongside structural models for the cubic γ phase with regular and inverse Heusler-type arrangements, respectively; all energies refer to absolute zero temperature, and the energy scale is referenced to the minimum of the hexagonal α phase, which is set to zero. The γ

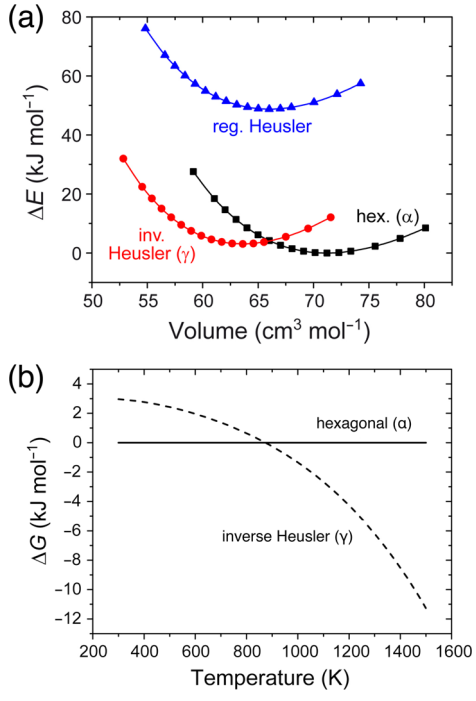

Figure 6. (a) Energy–volume data for α-Na_2MgPb with the Li_2CuAs-type structure (■), γ-Na_2MgPb with regular (▲) and inverse (●) Heusler-type structures. Lines are only guides to the eye. (b) Difference of the Gibbs free energy (ΔG) between hexagonal α-Na_2MgPb (—) and cubic γ-Na_2MgPb with the inverse Heusler-type structure (···) as a function of the temperature. The Gibbs free energy of the α-Na_2MgPb phase is set to zero.

dx.doi.org/10.1021/ic500466w | Inorg. Chem. 2014, 53, 5253–5259

phase with the inverse Heusler-type structure has a minimum value of +3.1 kJ mol^{-1}, being slightly less stable at 0 K than the α phase with the Li_2CuAs structure type (0 kJ mol^{-1}), but significantly more stable than a hypothetical γ phase with the regular Heusler-type structure (+48.8 kJ mol^{-1}).

The predicted ground-state molar volume of the γ phase with the inverse Heusler-type structure (63.6 cm^3 mol^{-1}) is 11% smaller than the value of the α phase (71.2 cm^3 mol^{-1}). The difference between the computed values is close to the experimentally determined molar volume difference of 9% between the γ phase (64.6 cm^3 mol^{-1}) and the α phase (70.8 cm^3 mol^{-1}) measured at 543 K.

The stability of the hexagonal α phase and the cubic γ phase with the inverse Heusler-type structure at high temperature may be evaluated to a higher degree of realism by invoking *ab initio* thermochemical computations based on lattice vibrations: this allows us to compare the temperature-dependent Gibbs free energies depicted in Figure 6b (see details in Supporting Information, Figure S2 and Table S2). Herein, the Gibbs energy of the α phase is set to zero. The Gibbs free energies of formation from the elements (ΔG_f) of the α phase and the γ phase at 298 K were obtained to be −47.96 and −44.99 kJ mol^{-1}, respectively. The difference in the Gibbs free energy between both phases is 3 kJ mol^{-1} at 298 K and decreases with increasing temperature, and then reaches to zero at around 900 K. The γ phase was indicated to be stable above 900 K. The experimental results revealed that the γ phase is the most stable above 533 K. The difference between the calculated and the experimentally measured temperatures for the phase stability may depend to some extent on technical details of the computations, as seen in other compounds before;[38] the important conclusion here is of a *qualitative* nature, and it readily supports the intuitive notion of the higher-symmetry (cubic) structure being more stable at high temperature than the lower-symmetry (hexagonal) alternative, and vice versa.

3.5. Electrical Properties. Figure 7 shows the temperature dependence of the electrical resistivity measured for a sintered sample of Na_2MgPb. The relative density of the sample was 70% of the theoretical density of the α phase. The electrical resistivity of the sample was 0.39 mΩ cm at 300 K and increased with increasing temperature to 491 K, and dropped at 491 and 521 K. An abrupt increase of the resistivity was observed at temperatures between 491 and 479 K on cooling.

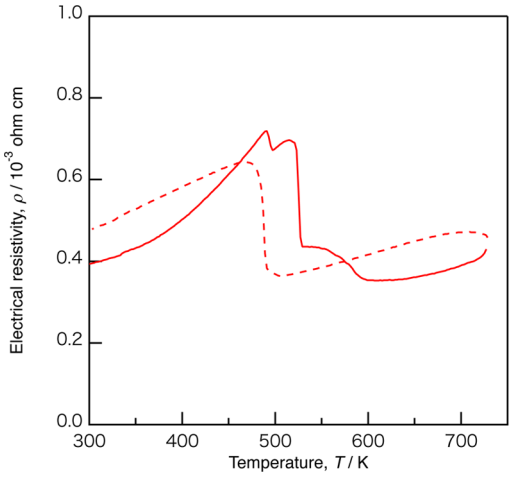

Figure 7. Electrical resistivity of the polycrystalline sample of Na_2MgPb. The data were measured on heating (solid line) and cooling (broken line).

The temperatures at which the resistivity dropped on heating were in good agreement with the temperatures at which the diffraction peaks of the β phase (493 K) and the γ phase (533 K) appeared in the high-temperature XRD patterns. Since the polycrystalline sample of $Na_{15}Pb_4$, which was an impurity phase in the Na_2MgPb sample, showed no abrupt change in the resistivity (Supporting Information Figure S4), the resistivity drops of the Na_2MgPb sample can be attributed to the structural phase transitions from α to β and from β to γ. The abrupt change of the resistivity on cooling was probably due to the structural phase transition from the high-temperature γ phase to the α phase because the sample after heating and cooling to room temperature had been seen to be the α phase as confirmed by powder XRD (Figure 3). No clear indication of the β phase formation was observed in the resistivity on cooling.

The measured electrical properties are also in sound qualitative agreement with electronic-structure computations, the results of which are given as Supporting Information. The computed electronic densities-of-states (DOS) of α-Na_2MgPb exhibit a narrow valley around the Fermi level; inspection of the band structure indicates gap closure at the Γ point. By contrast, the electronic DOS of γ-Na_2MgPb in the inverse Heusler-type structure indicates a higher amount of states at ε_F resulting from several band crossings, which is in line with the higher electrical conductivity observed for the γ phase.

4. CONCLUSIONS

The novel plumbide Na_2MgPb was prepared by heating the elements. The compound takes three different polymorphs depending on the temperature: a phase stable at room temperature, dubbed "α" phase, crystallizes in a Li_2CuAs-type structure (hexagonal, $P6_3/mmc$, Z = 2, a = 5.110(2) Å, c = 10.171(4) Å at 293 K); it transforms to a hexagonal ("β") phase from 493 to 553 K, and then the β phase to a cubic ("γ") phase from 533 to 633 K. The crystal structures of the β and γ phases could not be fully clarified by high-temperature XRD, although the cell parameters and molar volumes have been obtained. The $\beta \rightarrow \gamma$ transition is accompanied by a negative volume change of about 13−14%.

Ab initio calculations using density functional theory suggested that the inverse Heusler-type structure is a plausible structure model for the γ phase in comparison to the regular Heusler-type structure. The difference in calculated Gibbs free energies between the α phase and the γ phase indicates that the α phase is stable below 900 K, which qualitatively corroborates the experimental observation of the phase transition.

The temperature dependence of the electrical resistivity measured for the polycrystalline sample of Na_2MgPb indicated metallic-like behavior below 491 K, although the absolute value of the resistivity is higher than in common metals. The resistivity drops observed at 491 and 521 K on heating were due to the structural phase transitions from the α phase to the β phase and then from the β phase to the γ phase.

■ ASSOCIATED CONTENT

Supporting Information

X-ray crystallographic data in CIF format, additional structural information, results of phonon computations (indicating dynamic stability of both α and γ-Na_2MgPb), and electrical resistivity of the polycrystalline sample of $Na_{15}Pb_4$. This

dx.doi.org/10.1021/ic500466w | Inorg. Chem. 2014, 53, 5253−5259

material is available free of charge via the Internet at http://pubs.acs.org.

AUTHOR INFORMATION

Corresponding Author

*E-mail: yamataka@tagen.tohoku.ac.jp. Phone/fax: +81-22-217-5813.

Notes

The authors declare no competing financial interest.

ACKNOWLEDGMENTS

This work was supported in part by a Grant-in-Aid for Scientific Research (C) (No. 23550222) from the Ministry of Education, Culture, Sports, Science and Technology of Japan. V.L.D. gratefully acknowledges a scholarship from the Studienstiftung des deutschen Volkes (German National Academic Foundation). T.I. acknowledges the financial support by a Grant-in-Aid (No. 24350110) from JSPS, Japan.

REFERENCES

(1) Villars, P.; Cenzual, K. *Pearson's Crystal Data*, Release 2013/14; ASM International: Materials Park, Ohio, 2013.
(2) Schuster, H.-U. *Naturwissenschaften* **1966**, *53*, 361.
(3) Schuster, H.-U. *Z. Anorg. Allg. Chem.* **1969**, *370*, 149−159.
(4) Schönemann, H.; Jacobs, H.; Schuster, H.-U. *Z. Anorg. Allg. Chem.* **1971**, *382*, 40−48.
(5) Kuriyama, K.; Yahagi, M.; Iwamura, K. *Jpn. J. Appl. Phys.* **1973**, *12*, 743−744.
(6) Schönemann, H.; Schuster, H.-U. *Rev. Chim. Miner.* **1976**, *13*, 32−40.
(7) Matthes, R.; Schuster, H.-U. *Z. Naturforsch., B* **1978**, *33*, 115−117.
(8) Pobitschka, W.; Schuster, H.-U. *Z. Naturforsch., B* **1978**, *33*, 115−117.
(9) Matthes, R.; Schuster, H.-U. *Z. Naturforsch., B* **1980**, *35*, 778−780.
(10) Cullmann, H.-O.; Hinterkeuser, H. W.; Schuster, H.-U. *Z. Naturforsch., B* **1981**, *36*, 917−921.
(11) Cullmann, H.-O.; Schuster, H.-U. *Z. Anorg. Allg. Chem., B: Anorg. Chem., Org. Chem.* **1986**, *537*, 7−16.
(12) Lacroix-Orio, L.; Tillard, M.; Belin, C. *Solid State Sci.* **2006**, *8*, 208−215.
(13) Cheviré, F.; DiSalvo, F. J. *Acta Crystallogr., Sect. E* **2007**, *63*, i62−i63.
(14) Pauly, H.; Weiss, A.; Witte, H. *Z. Metallkd.* **1968**, *59*, 414−418.
(15) Ramsey, W. J. *Acta Crystallogr.* **1961**, *14*, 1092−1093.
(16) Teslyuk, M. Y.; Mel'nyk, E. V.; Malinkovich, A. N.; Mitrofanova, M. F. *Visn. L'Viv. Derzh. Univ., Ser. Khim.* **1969**, *11*, 25−30.
(17) Becka, L. N.; Cruickshank, D. W. J. *Ukr. Khim. Zh.* **1992**, *58*, 735−737.
(18) Herbst, J. F.; Meyer, M. S. *J. Alloys Compd.* **2010**, *492*, 65−68.
(19) Yamada, T.; Deringer, V. L.; Dronskowski, R.; Yamane, H. *Inorg. Chem.* **2012**, *51*, 4810−4816.
(20) *PROCESS-AUTO*; Rigaku/MSC & Rigaku Corporation: The Woodlands, TX, 2005.
(21) Higashi, T. *NUMABS—Numerical Absorption Correction*; Rigaku Corporation: Tokyo, 1999.
(22) Sheldrick, G. M. *Acta Crystallogr., Sect. A* **2008**, *64*, 112−122.
(23) Farrugia, L. J. *J. Appl. Crystallogr.* **1999**, *32*, 837−838.
(24) Gelato, L. M.; Parthé, E. *J. Appl. Crystallogr.* **1987**, *20*, 139−143.
(25) (a) Kresse, G.; Hafner, J. *Phys. Rev. B* **1993**, *47*, 558−561. (b) Kresse, G.; Furthmüller, F. *Comput. Mater. Sci.* **1996**, *6*, 15−50.
(26) (a) Kresse, G.; Furthmüller, J. *Phys. Rev. B* **1996**, *54*, 11169−11186. (b) Kresse, G.; Joubert, D. *Phys. Rev. B* **1999**, *59*, 1758−1775.
(27) Mermin, N. D. *Phys. Rev. A* **1965**, *137*, 1441−1443.
(28) Blöchl, P. E. *Phys. Rev. B* **1994**, *50*, 17953−17979.
(29) Perdew, J. P.; Burke, S.; Ernzerhof, M. *Phys. Rev. Lett.* **1996**, *77*, 3865−3868.
(30) Blöchl, P. E.; Jepsen, O.; Andersen, O. K. *Phys. Rev. B* **1994**, *49*, 16223−16233.
(31) Monkhorst, H. J.; Pack, J. D. *Phys. Rev. B* **1976**, *13*, 5188−5192.
(32) Parlinski, K.; Li, Z. Q.; Kawazoe, Y. *Phys. Rev. Lett.* **1997**, *78*, 4063−4066.
(33) Togo, A.; Oba, F.; Tanaka, I. *Phys. Rev. B* **2008**, *78*, 134106−1−9.
(34) Stoffel, R. P.; Wessel, C.; Lumey, M.-W.; Dronskowski, R. *Angew. Chem., Int. Ed.* **2010**, *49*, 5242−5266.
(35) Clementi, E.; Raimondi, D. L. *J. Chem. Phys.* **1963**, *38*, 2686−2689.
(36) Honig, R. E.; Kramer, D. A. *RCA Rev.* **1969**, *30*, 285−305.
(37) Schuster and Schönemann reported that Li_2ZnGe has a BiF_3-type structure with $Fm\bar{3}m$ on the basis of powder XRD analysis in refs 3 and 6. Recently, however, Laroix-Orio et al. redetermined the crystal structure of Li_2ZnGe and found the inverse Heusler-type structure through single-crystal structural analysis in ref 12.
(38) Deringer, V. L.; Lumeij, M.; Stoffel, R. P.; Dronskowski, R. *J. Comput. Chem.* **2013**, *34*, 2320−2326.